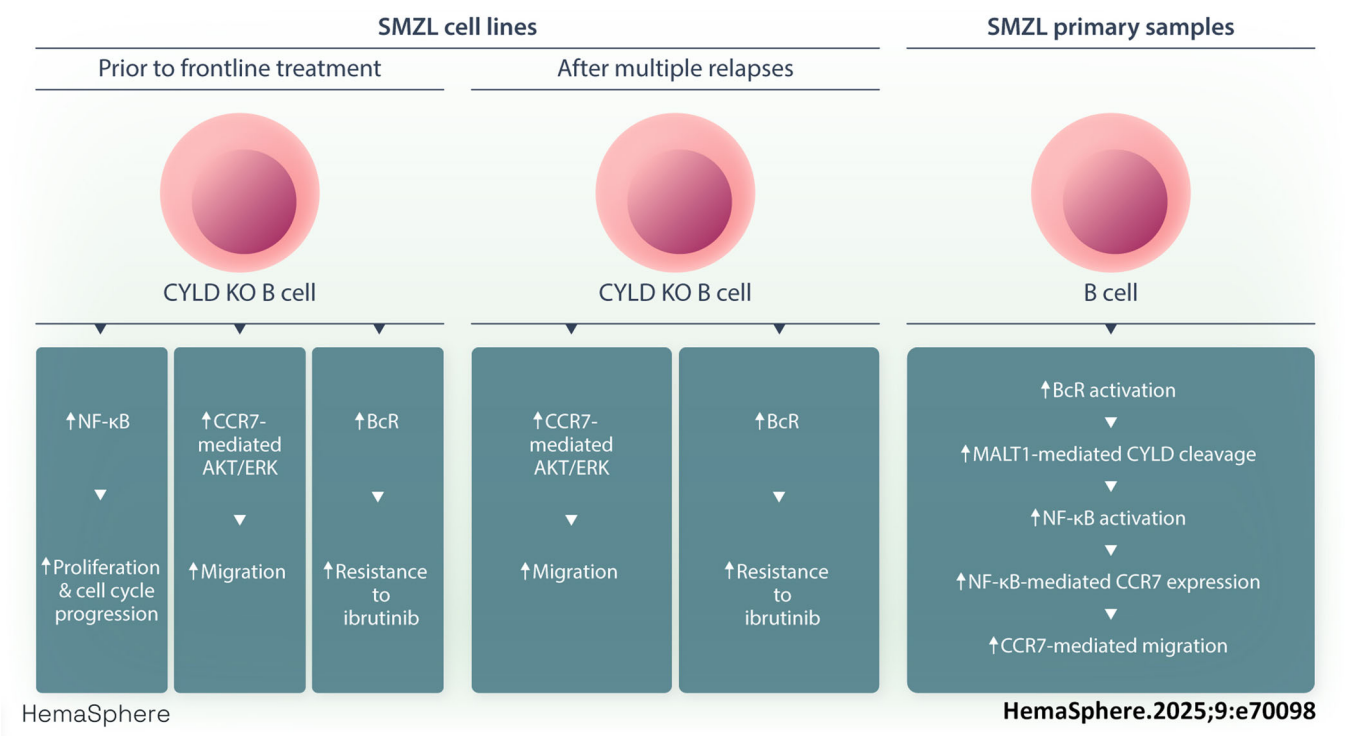




Loss of CYLD promotes splenic marginal zone lymphoma

Athanasios Pseftogas^{1,2}  | Jessica Bordini² | Silvia Heltai¹ |
Ferdinando Bonfiglio^{3,4} | Georgios Gavriilidis⁵ | Vasileios Vasileiou^{5,6} |
Sofoklis Keisaris⁵ | Daniela Belloni^{1,2} | Caterina Taccetti⁷ | Pamela Ranghetti² |
Eleonora Perotta² | Michela Frenquelli² | Uday Aditya Sarkar⁸ | Elisa Albi² |
Francesca Martini² | Emanuela Sant'Antonio² | Fabrizio Mavilia² |
Fotis Psomopoulos⁵ | Manasori Daibata⁹ | José Ángel Martínez Climent¹⁰ |
George Mosialos¹¹ | Davide Rossi¹² | Alessandro Campanella¹ | Lydia Scarfò^{1,2} |
Kostas Stamatopoulos⁵ | Konstantinos Xanthopoulos¹¹ | Paolo Ghia^{1,2} 

Graphical Abstract



Loss of CYLD promotes splenic marginal zone lymphoma

Athanasios Pseftogas^{1,2}  | Jessica Bordini² | Silvia Heltai¹ |
 Ferdinando Bonfiglio^{3,4} | Georgios Gavriilidis⁵ | Vasileios Vasileiou^{5,6} |
 Sofoklis Keisaris⁵ | Daniela Belloni^{1,2} | Caterina Taccetti⁷ | Pamela Ranghetti² |
 Eleonora Perotta² | Michela Frenquelli² | Uday Aditya Sarkar⁸ | Elisa Albi² |
 Francesca Martini² | Emanuela Sant'Antonio² | Fabrizio Mavilia² |
 Fotis Psomopoulos⁵ | Manasori Daibata⁹ | José Ángel Martínez Climent¹⁰ |
 George Mosialos¹¹ | Davide Rossi¹² | Alessandro Campanella¹ | Lydia Scarfò^{1,2} |
 Kostas Stamatopoulos⁵ | Konstantinos Xanthopoulos¹¹ | Paolo Ghia^{1,2} 

Correspondence: Athanasios Pseftogas (pseftogas.athanasio@hsr.it); Paolo Ghia (ghia.paolo@hsr.it)

Abstract

Splenic marginal zone lymphoma (SMZL) is a distinct clinical and pathological entity among marginal zone lymphomas. Genetic and microenvironmental factors leading to aberrant activation of the NF- κ B pathway have been implicated in SMZL pathogenesis. CYLD is a negative regulator of NF- κ B and other signaling pathways acting as a deubiquitinase of regulatory molecules and has been reported as a tumor suppressor in different types of cancer, including B-cell malignancies. To assess whether CYLD is implicated in the natural history of SMZL, we profiled primary cells from patients with SMZL and SMZL cell lines for CYLD expression and functionality. We report that CYLD is downregulated in patients with SMZL and that CYLD ablation in vitro leads to NF- κ B pathway hyperactivation, promoting the proliferation of SMZL cells. In addition, we found that CYLD deficiency was associated with increased migration of SMZL cells in vitro, through CCR7 receptor signaling, and with increased dissemination in vivo. CYLD loss was sufficient to induce BcR signaling, conferring increased resistance to ibrutinib treatment in vitro. In summary, our work uncovers a novel role of CYLD as a key regulator in SMZL pathogenesis, dissemination, and resistance to targeted agents. On these grounds, CYLD could be proposed as a novel target for patient stratification and personalized interventions.

INTRODUCTION

Splenic marginal zone lymphoma (SMZL) is a distinct subtype of marginal zone lymphoma, characterized by splenomegaly and lymphocytosis. SMZL comprises <2% of all lymphoid malignancies and is typically diagnosed at an advanced age.¹ SMZL is highly heterogeneous and this heterogeneity appears to be due to a complex interplay between genetic aberrations and microenvironmental factors involved in shaping its natural history. From a genetic standpoint,

SMZL is characterized by gene mutations in NF- κ B pathway regulators,² Notch pathway components,³ and *KLF2*⁴ as well as by a pronounced bias to the expression of clonotypic B cell receptors (BcR) using the IGHV1-2*04 gene.⁵

In terms of microenvironmental clues, stimulation of both the BcR and the TLRs induces MAPK and NF- κ B signaling pathway activation, which has a central role in the expansion of the neoplastic clone.⁶ Interestingly, the identification in SMZL patients of distinct mutations in genes downstream of the BcR and TLR signaling

¹Università Vita-Salute San Raffaele, Milano, Italy

²IRCCS Ospedale San Raffaele, Milano, Italy

³University of Naples Federico II, Napoli, Italy

⁴CEINGE Biotecnologie avanzate s.c.a r.l., Napoli, Italy

⁵CERTH, Thessaloniki, Greece

⁶Democritus University of Thrace, Alexandroupolis, Greece

⁷IFOM, the FIRC Institute of Molecular Oncology, Milano, Italy

⁸Dana-Farber Cancer Institute, Boston, Massachusetts, USA

⁹Kochi Medical School, Kochi, Japan

¹⁰Cima University, Navarra, Spain

¹¹Aristotle University of Thessaloniki, Thessaloniki, Greece

¹²The Oncology Institute of Southern Switzerland, Bellinzona, Switzerland

This is an open access article under the terms of the [Creative Commons Attribution-NonCommercial-NoDerivs](https://creativecommons.org/licenses/by-nc-nd/4.0/) License, which permits use and distribution in any medium, provided the original work is properly cited, the use is non-commercial and no modifications or adaptations are made.

© 2025 The Author(s). *HemaSphere* published by John Wiley & Sons Ltd on behalf of European Hematology Association.

pathways, including NF- κ B signaling, further underscores the relevance of these pathways in disease pathogenesis.⁷ Notably, activation of these pathways, regardless of the presence of mutations, has helped recently to better stratify SMZL into two distinct groups, termed NKK (characterized by NF- κ B, Notch, and KLF2 signaling) and DMT (characterized by DNA-damage response, MAPK, and TLR signaling).⁸ Additionally, based on the type of immune microenvironment, SMZL was segregated into an “immune-suppressive” subgroup, associated with inflammation and immune checkpoint activation signatures, and an “immune-silent” subgroup, characterized by an immune-excluded phenotype.⁸

CYLD is a predominantly cytoplasmic deubiquitinase, hydrolyzing K63-linked and linear polyubiquitin chains. Such ubiquitination patterns do not mediate protein degradation but instead, serve as scaffolds for the assembly of protein complexes that mediate the activation of protein kinases, such as TAK1 and IKK.⁹ Through deubiquitination of key molecules, CYLD acts as a negative regulator of NF- κ B, JNK, p38,¹⁰ Wnt, and Notch¹¹ pathways.

CYLD was originally described as a tumor suppressor that is causally associated with the development of tumors in skin appendages.¹² Increasing evidence suggests a potential role in B cell lymphoproliferative disorders: (i) CYLD expression is downregulated in chronic lymphocytic leukemia (CLL)¹³ and classical Hodgkin lymphoma¹⁴; (ii) somatic mutations in the CYLD gene have been identified in multiple myeloma¹⁵ and, (iii) in MALT lymphomas, the MALT1-API2 oncogenic complex targets A20 and CYLD deubiquitinases for NF- κ B activation.¹⁶ More recently, MALT1-mediated CYLD cleavage was implicated in Bcr-signaling, NF- κ B activation, and proliferation in mantle cell lymphoma (MCL) and diffuse large B-cell lymphoma (DLBCL)¹⁷, while it was also reported that BTK inhibitors induce apoptosis in non-GCB-DLBCL by decreasing CYLD phosphorylation.¹⁸

NF- κ B and Notch signaling pathways as well as the KLF2 transcription factor are key factors that regulate the generation and differentiation of marginal zone B cells¹⁹ while deregulation of both the canonical and the non-canonical NF- κ B signaling pathways is a common finding in all marginal zone lymphoma subtypes.²⁰ Considering that CYLD is a negative regulator of NF- κ B and Notch signaling pathways and, in SMZL, KLF2 mutations impair its ability to suppress NF- κ B activation induced by various stimuli,⁴ we hypothesized that CYLD may have a central role in SMZL pathogenesis.

In this study, taking advantage of both primary samples from patients with SMZL and human SMZL cell lines, we show that CYLD loss leads to increased proliferation, dissemination, and resistance to the treatment with the BTK inhibitor ibrutinib, being envisioned as a potential new biomarker that may help stratify the patients toward more personalized treatments.

METHODS

Cell lines and reagents

SMZL cell lines, SL-15²¹ and SL-22,²² were generously provided by Dr. Masanori Daibata. They were cultured in RPMI-1640 (#ECB2000L, EuroClone) supplemented with 10% fetal bovine serum (#ECS5000L, EuroClone), 100 U/mL penicillin, and 100 mg/mL streptomycin (#ECB3001D, EuroClone) and maintained at 37°C in a humidified atmosphere with 5% CO₂. HUVEC cells were cultured in EGM™-2 Endothelial Cell Growth Medium-2 BulletKit™ (#CC-3162, Lonza) and maintained at 37°C in a humidified atmosphere with 5% CO₂. Cell line authentication was carried out by using eight different and highly polymorphic short tandem repeat (STR) loci (DSMZ, Braunschweig, Germany) and the cell lines were routinely tested for mycoplasma contamination using PCR.

The BTK inhibitor ibrutinib was purchased from Selleckchem (#PCI-32765) and the MALT1 inhibitor MI-2 was purchased from MedChemExpress (#HY-12276). Mouse anti-hCCR7 mAb (#MAB197, 150503 clone, IgG2a) and the respective isotype control (#MAB003, IgG2a) were purchased from R&D Systems.

Patient samples

Primary peripheral blood and bone marrow samples were collected from 21 patients with SMZL after routine diagnostics at IRCCS Ospedale San Raffaele; Milano, Italy; clinical information about the studied cases is summarized in Supporting Information S1: Table S1. This study was approved by the San Raffaele Committee on Human Experimentation and informed consent was obtained in accordance with the revised Declaration of Helsinki 2008. Forty-four fresh biopsy spleen samples and 246 spleen FFPE biopsy samples were previously collected and analyzed in the context of the IELSG46 study as described⁸ (Supporting Information S1).

Generation of CYLD-deficient SL-15 and SL-22 cell lines

Generation of the stable CYLD-deficient SL-15 and SL-22 cell lines was performed as previously described.²³ Briefly, two sgRNAs targeting exons 2 and 9 of the CYLD locus and one control sgRNA targeting GFP, were subcloned in the LentiCRISPRv2 vector. All sgRNA sequences are listed in Supporting Information S1: Table S2. The SL-15 and SL-22 cell lines were transduced with lentiviral supernatants and, after puromycin selection, monoclonal cell colonies were subcultured and established. The CYLD-deficient clones KO-E2 (SL-15) and KO-C6 (SL-22) were generated with sgRNA targeting exon 2, while the CYLD-deficient clones KO-H11 (SL-15) and KO-E7 (SL-22) were generated with sgRNA targeting exon 9.

Cell proliferation assay

Control (CTL) and CYLD knockout (KO) SL-15 and SL-22 cells were seeded in a 12-well cell culture plate (10⁵ cells/well) in 1 mL of RPMI 1640 (Euroclone) and cell viability was determined every 24 h until 96 h by MTT (#475 989, Sigma-Aldrich) and Trypan Blue exclusion assay (#T8154, Sigma-Aldrich) using TC10 Automated Cell Counter (Bio-Rad). For the MTT assay, the absorbance was measured at 570 nm using a Perkin Elmer Wallac Victor 1420 multilabel counter. For patients with SMZL, PBMCs were seeded in a 96-well plate at 5 × 10⁵ cells/well and treated with vehicle (DMSO) or MI-2 (1 μ M) for up to 72 h.

Cell cycle assay

4 × 10⁵ control (CTL) and CYLD knockout (KO) SL-15 and SL-22 cells were seeded on a 6-well plate in 2 mL of R10 medium with 2 mM thymidine (#T1895, Sigma-Aldrich) for 18 h. Then, cells were washed with RPMI medium and seeded again on a six-well plate without thymidine for 9 h. For completing synchronization, cells were treated again with 2 mM thymidine for 16 h. Next, cells were washed twice with PBS and stained with 5 μ L Propidium Iodide (#00-6990, Invitrogen). Flow cytometry was performed on a Navios Beckman Coulter flow cytometer and the cell cycle was analyzed with FCS Express Version 7 software.

Ibrutinib treatment and cell proliferation assay

Parental SL-15 and SL-22 cell lines, as well as control (CTL) and CYLD knockout (KO) SL-15 and SL-22 cells, were seeded in a 12-well cell culture plate (10^5 cells/well) in 1 mL of RPMI 1640 (Euroclone) and treated with either DMSO or 1, 2.5, 5, 10, and 20 μ M of Ibrutinib for up to 72 h. Cell viability was evaluated by Trypan Blue exclusion and CellTiter-Glo Luminescent assay (#G7570, Promega) every 24 h. The results were expressed as a percentage of viability calculated by the ratio between the number of live cells treated with ibrutinib and the number of live cells treated with vehicle (DMSO). Ibrutinib IC₅₀ value was calculated using a nonlinear regression tool from GraphPad Prism Version 9 software.

Transwell migration assay

Migration capacity was evaluated using Transwell chambers (6.5 mm diameter, 10 μ m thickness, and 5 μ m diameter pore size, Corning-Costar). Briefly, control (CTL) and CYLD knockout (KO) SL-15 and SL-22 cells were seeded in the upper chamber (3×10^5 cells/chamber) in 0.2 mL of RPMI 1640 (Euroclone). When required, cells were pre-treated before seeding with 10 μ g/mL of mouse anti-hCCR7 mAb (#MAB197, 150503 clone, IgG2a) or the respective isotype control (#MAB003, IgG2a) for 4 h. Then, 0.6 mL of RPMI 1640 with or without 200 ng/mL of CCL19 (#300-29B, Peprotech) or CCL21 (#300-35A, Peprotech) chemokines were added to the lower compartment and plates were incubated at 37°C in 5% CO₂. After 16 h of incubation, migrated cells on the lower chamber were collected, stained with anti-CD19-FITC (#A07768, Beckman-Coulter), and counted for 60 s using a BD FACS Canto II flow cytometer.

Transendothelial migration (TEM) assay

Migration capacity after bypassing vascular endothelium was evaluated by seeding 10^5 HUVEC cells in the gelatin-coated upper chamber of Transwell chambers (6.5 mm diameter, 10 μ m thickness, and 5 μ m diameter pore size, Corning-Costar) in 0.2 mL of complete EGM2 medium (Lonza). As a control for determining the confluency status, the same number of HUVEC cells were seeded in three wells of a 96-well tissue culture plate (Corning-Costar). Plates were then incubated at 37°C in a humidified atmosphere with 5% CO₂ until HUVEC cells reached 100% confluency. Confluent monolayers were stimulated with 40 ng/mL recombinant TNF α (#300-01A, Peprotech) for 6 h prior to assay initiation. After HUVEC cell activation and medium respiration, control (CTL) and CYLD knockout (KO) cells of SL-15 and SL-22 cell lines or PBMCs isolated from patients with SMZL, were seeded in the upper chamber (3×10^5 cells/chamber) in 0.2 mL of RPMI 1640 (Euroclone). When required, cells were pre-treated before seeding with 10 μ g/mL of mouse anti-hCCR7 mAb (#MAB197, 150503 clone, IgG2a) or the respective isotype control (#MAB003, IgG2a) for 4 h. For patients with SMZL, PBMCs were pre-treated with DMSO (vehicle) or 1 μ M of MI-2 for 6 h. Lower compartments were then filled with 0.6 mL of RPMI 1640 with or without 200 ng/mL of CCL19 (#300-29B, Peprotech) or CCL21 (#300-35A, Peprotech) chemokines, and the plates were incubated at 37°C in 5% CO₂. After 16 h of incubation, cells of the lower chamber were collected, stained with anti-CD19-FITC (#A07768, Beckman-Coulter), and counted for 60 s using a BD FACS Canto II flow cytometer.

RNA sequencing of primary SMZL samples

RNA-seq (TruSeq Stranded mRNA Kit, Illumina) of 44 fresh biopsy samples previously collected⁸ was used to investigate CYLD expression in tumor and control spleens. Gene expression was also assessed in 246 spleen FFPE biopsy samples previously collected,⁸ using HTG EdgeSeq Precision Immuno-Oncology (HTG-PIO) and HTG EdgeSeq Oncology Biomarker Panels (HTG-OBP). Sequencing data was processed as described in Bonfiglio et al.,⁸ and microenvironment cluster labels (immune-suppressive and immune-silent clusters) were adopted from the original publication.⁸ More specifically, 16 gene expression signatures of distinct microenvironmental cell populations and states and in situ profiling were used to define the two microenvironment clusters.⁸ Differences in gene expression were tested with a two-sided Student's *t*-test. We subdivided the FFPE cohort into two groups (high CYLD, low CYLD) according to the median of CYLD gene expression and performed a relative survival analysis, defined as the ratio between survival observed in patients and expected survival of the general population matched to by geographical origin, sex, age, and calendar year of diagnosis, using the Ederer II method.²⁴

Statistical analysis

All data sets were taken from $n \geq 3$ biological replicates unless mentioned otherwise. Data are presented as mean \pm SEM. Analyses were performed using GraphPad Prism Version 9 software for Student's *t*-test or two-way ANOVA followed by Fisher's test. Analysis of categorical variables was done using the χ^2 test and Fisher's exact test when appropriate and $p < 0.05$ was considered statistically significant.

Further details on experimental procedures are provided in the Supporting Information S1: Methods section.

RESULTS

CYLD is downregulated in patients with SMZL and associates with inferior relative survival

Differential analysis of our previously published data⁸ comparing spleen samples of 35 patients with SMZL versus nine normal individuals revealed a significant ($p = 4.4 \times 10^{-8}$) reduction of CYLD expression (Figure 1A), with no difference between the NKK and DMT subtypes of SMZL (data not shown). That said, CYLD expression levels correlated with relative survival: 125 patients from the IELSG cohort with CYLD expression below the median (low CYLD group) had a 10-year life expectancy of 81.3% ($p = 1.0 \times 10^{-4}$) compared to a general population matched by age, gender, country of origin and calendar year of diagnosis (Figure 1B). In contrast, 87 patients from the same cohort with CYLD expression above the median (high CYLD group) had a 10-year life expectancy of 90.1%, not significantly different from the matched general population ($p = 0.16$, Figure 1B). Interestingly, CYLD was downregulated in patients with SMZL characterized by an "immune-suppressive" microenvironment (associated with inflammation and immune checkpoint activation signatures and associated with more aggressive disease⁸) when compared to the "immune-silent" counterparts ($p = 3.2 \times 10^{-14}$, Figure 1C). Intriguingly, there was a trend to decreased overall survival in CYLD^{low} compared to CYLD^{high} groups, though the difference was not statistically significant (Supporting Information S1: Figure S1).

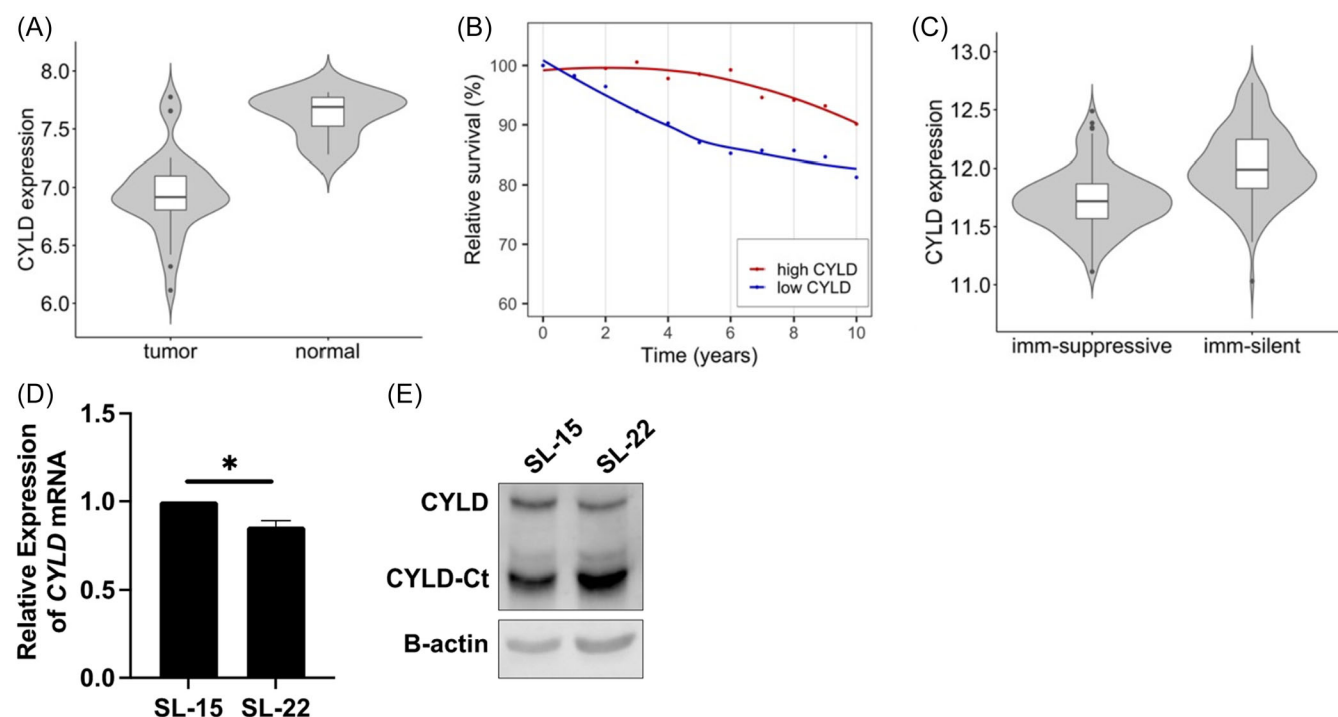


FIGURE 1 Variable CYLD expression in SMZL patients and cell lines. (A) Violin plot of CYLD expression in tumor ($n = 35$) and normal ($n = 9$) samples from fresh spleen biopsies. (B) Relative survival rates (RS rates) are shown for the high CYLD and low CYLD subgroups. (C) Violin plot of CYLD expression in FFPE samples stratified by different microenvironmental classes. (D) RT-qPCR analysis of CYLD mRNA expression in SMZL cell lines. Values are shown as the mean \pm SEM of relative mRNA levels from at least three independent experiments. Data were normalized to CYLD expression of the SL-15 cell line. Statistical analysis was performed by the Student's t -test method (* $p < 0.05$). (E) Representative picture of immunoblot analysis of CYLD protein expression in whole cell extracts from the SMZL cell lines. For CYLD analysis, we used an antibody that recognized both the full-length CYLD and a C-terminal fragment of CYLD (CYLD-Ct). B-actin was used as a loading control. The picture is representative of three independent experiments.

CYLD ablation leads to NF- κ B signaling activation and increased proliferation in SMZL cell lines

To investigate the role of CYLD in SMZL, we assessed CYLD mRNA and protein levels in the SL-15 and SL-22 SMZL cell lines, established from circulating cells of a patient with SMZL prior to frontline treatment²¹ and after multiple relapses.²² We observed significantly ($p < 0.05$) reduced CYLD mRNA and protein levels (Figure 1D,E) in SL-22 versus SL-15 cells, which was accompanied by increased cleavage of CYLD (Figure 1E, CYLD-Ct band). To dissect the role of CYLD in SMZL cells, we established control (CTL) and CYLD knockout (KO) monoclonal populations of the SL-15 and SL-22 cell lines (Figure 2A). CYLD ablation led to increased activation of both canonical (p105/p50) and non-canonical (p100/p52) NF- κ B signaling pathways only in the SL-15 cell line, as assessed by elevated p105/p50 (Figure 2B,C) and p100/p52 (Figure 2D,E) as well as by the upregulation of well-known canonical (*IL6* and *CD80*) and non-canonical (*ICAM1*) NF- κ B target genes (Figure 2F and Supporting Information S1: Figure S2A). In addition, only SL-15 CYLD KO cells showed higher proliferation capacity compared to CTL (Figure 2G,H and Supporting Information S1: Figure S2B,C). Accordingly, cell cycle analysis revealed a higher progression of SL-15 CYLD KO cells into the S and G2/M phases, associated with *CDK1* and *CDK2* upregulation, in line with the observed proliferation status (Figure 2I and Supporting Information S1: Figure S3A).

CYLD ablation in SL-15 cells was associated with increased proliferation and a transcriptional program that was characterized by

higher *PLK1*, *CDK1*, *CDK2*, and *NOTCH2* and decreased *KLF2* expression levels, similar to the SL-22 cell line (Supporting Information S1: Figure S3A,B). Altogether, our findings support that loss of CYLD is associated with a higher proliferative potential, arguably linked to clinical aggressiveness.

CYLD ablation enhances the migration capacity of SMZL cells

The expression of chemokine receptors, including CCR7, is regulated by the NF- κ B and AP-1 transcription factors.²⁵ With this in mind, we investigated CCR7 expression levels in control and CYLD KO clones of the SL-15 and SL-22 cell lines and documented overexpression in the former (Figure 3A,B and Supporting Information S1: Figure S4A,B).

In order to explore the migration capacity of CTL and CYLD KO clones, we performed transwell and transendothelial migration assays in the presence or the absence of (i) CCL19/CCL21 chemokines, and (ii) an anti-CCR7 neutralizing antibody. In the absence of chemoattractant, CYLD KO clones of both SMZL cell lines migrated significantly more than CTL clones, but higher basal migration capacity was observed in SL-15 versus SL-22 cells, correlating with the elevated CCR7 expression levels in the former (Figure 3C and Supporting Information S1: Figure S4C). CYLD KO clones also showed *MMP9* overexpression (Figure 3D,E). The addition of CCL19/CCL21 ligands increased the number of migrated cells in all CTL and, in particular, in the CYLD KO clones (transendothelial migration assay

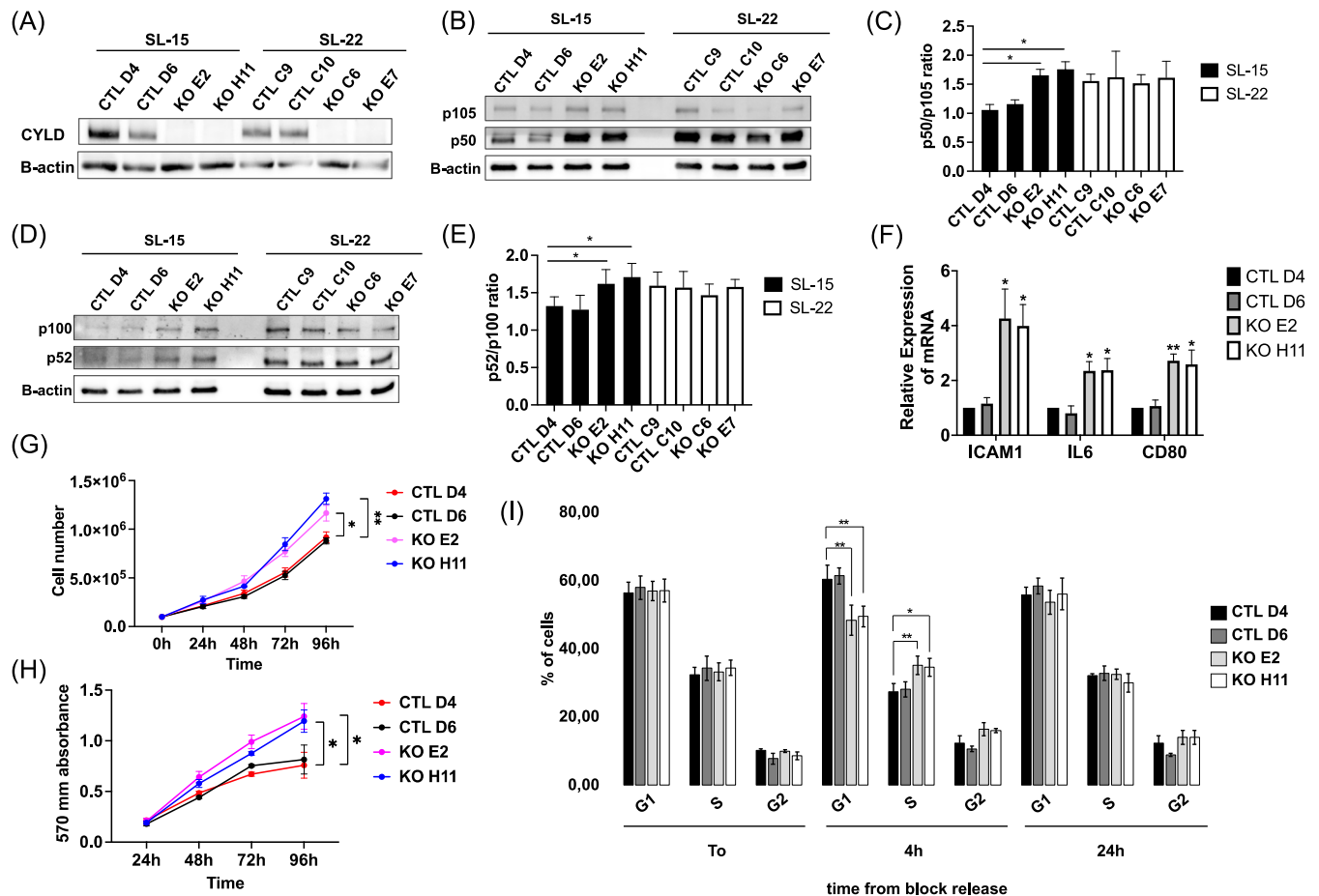


FIGURE 2 CYLD ablation induces NF-κB pathway activation, proliferation, and cell cycle progression of the SL-15 cell line. **(A)** Immunoblot analysis of CYLD protein expression in whole cell extracts from two control (CTL) and two CYLD KO (KO) clones of SL-15 and SL-22 cell lines. **(B)** Immunoblot analysis of p105-p50 (canonical NF-κB pathway) in whole cell extracts from two control (CTL) and two CYLD KO (KO) clones of SL-15 and SL-22 cell lines. The picture is representative of three independent experiments. **(C)** Quantification of p50/p105 ratio of immunoblot analysis presented in (B). Values are presented as the mean ± SEM of three independent experiments and statistical analysis was performed by Student's *t*-test (**p* < 0.05). **(D)** Immunoblot analysis of p100-p52 (non-canonical NF-κB pathway) in whole cell extracts from two control (CTL) and two CYLD KO (KO) clones of the SL-15 and SL-22 cell lines. The picture is representative of three independent experiments. **(E)** Quantification of p52/p100 ratio of immunoblot analysis presented in (D). Values are presented as the mean ± SEM of three independent experiments, and statistical analysis was performed by Student's *t*-test (**p* < 0.05). **(F)** RT-qPCR analysis of *CD80*, *IL6*, and *ICAM1* mRNA in two control (CTL) and two CYLD KO (KO) clones of the SL-15 cell line. Values are presented as the mean ± SEM of relative mRNA levels from at least three independent experiments. Data were normalized to the mRNA expression of the CTL D4 clone and statistical analysis was performed by Student's *t*-test (**p* < 0.05, ***p* < 0.01). **(G)**, **(H)** Proliferation analysis by Trypan blue exclusion assay (**G**) and MTT assay (**H**) of two control (CTL) and two CYLD KO (KO) clones of the SL-15 cell line, measured at 0, 24, 48, 72, and 96 h after seeding. Representative graph of three independent experiments, each performed in triplicate. Values are shown as the mean ± SEM, and statistical significance was assessed by the Student's *t*-test (**p* < 0.05, ***p* < 0.01). **(I)** Cell cycle analysis of two control (CTL) and two CYLD KO (KO) clones of the SL-15 cell line, 4 and 24 h after thymidine synchronization, assessed by flow cytometry after staining with propidium iodide (PI). Values are presented as the mean ± SEM of triplicate experiments, and statistical analysis was performed by Student's *t*-test (**p* < 0.05, ***p* < 0.01).

after CCL19 addition: CTL D4, from 1.3×10^3 to 2.1×10^3 ; KO E2, from 2.9×10^3 to 5.5×10^3 ; KO H11, from 2.2×10^3 to 5.1×10^3). Interestingly, initial neutralization of CCR7 blocked the chemokine-induced migratory capacity of CYLD KO clones near basal levels (Figure 3C and Supporting Information S1: Figure S4C). Mechanistically, the anti-CCR7 antibody attenuated the activation of the MEK/ERK1/2 and PI3K/AKT signaling cascades that are activated upon CCL19/CCL21 binding²⁶ (Figure 3F and Supporting Information S1: Figure S4D).

In order to evaluate the migration ability of CTL and CYLD KO clones *in vivo*, we injected the modified cell lines intravenously in Rag2^{-/-}γc^{-/-} immunodeficient mice and sacrificed them three weeks later. Tissue dissemination of each clone was evaluated based on the percentage of CD19⁺/CD45⁺ cells detected by flow cytometry after disaggregation of the organs. CYLD KO clones of both SL-15 and

SL-22 cell lines showed a higher percentage of CD19⁺ CD45⁺ B cells in all analyzed compartments (peripheral blood, liver, peritoneal cavity, and spleen; Figure 3G and Supporting Information S1: Figure S4E), except the bone marrow (data not shown). In addition, mice injected with CYLD KO clones exhibited heavier and larger spleens with tumor foci (Figure 3H,I and Supporting Information S1: Figure S4F,G).

To dissect the molecular effects of CYLD ablation in SMZL cell lines, we performed RNA-sequencing in control and CYLD KO clones of the SL-15 cell line. Differential expression (DE) analysis showed that CCR7 expression was significantly higher in CYLD KO clones versus control SL-15 cells (Supporting Information S1: Figure S5A). Gene Set Enrichment Analysis (GSEA) revealed that cytokine-mediated signaling pathway, positive regulation of ERK1/2 and NF-κB pathway, and regulation of protein phosphorylation were among

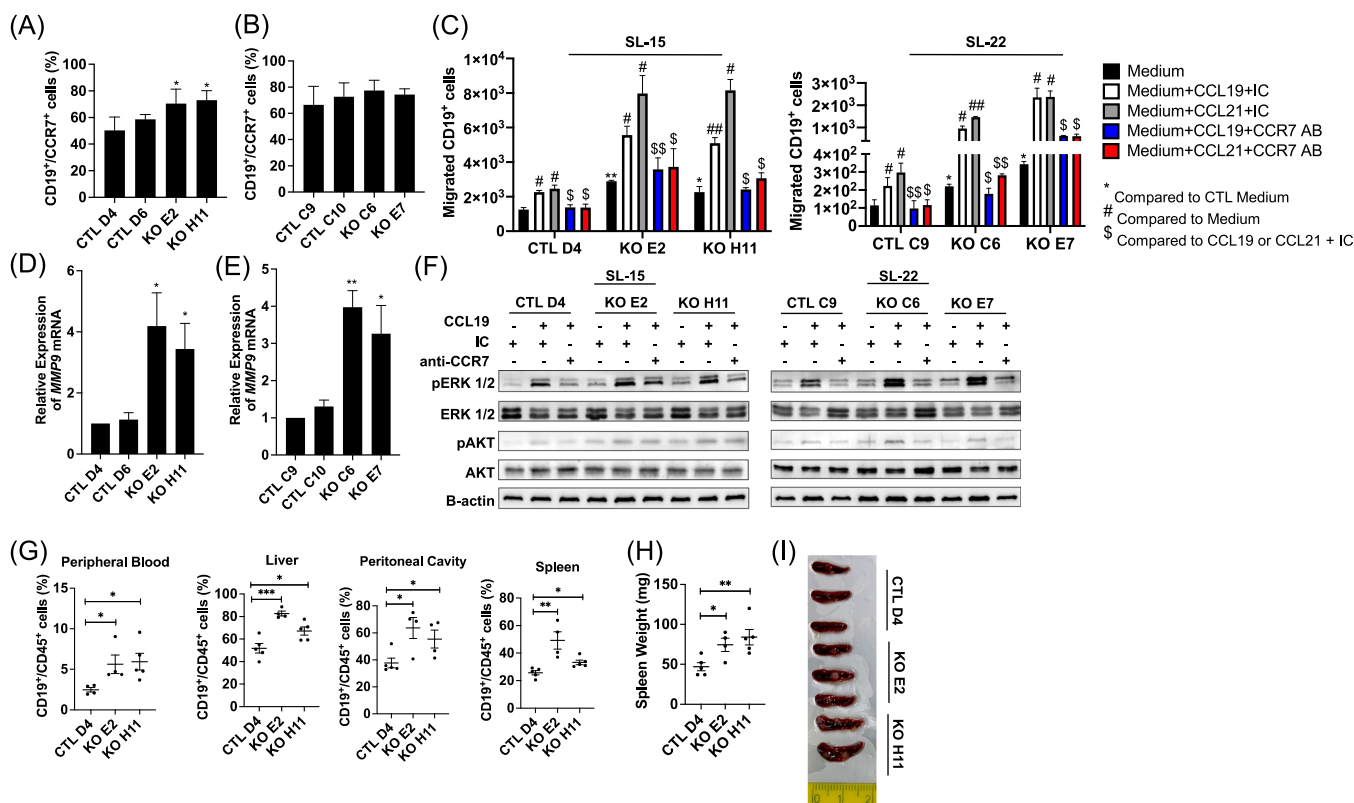


FIGURE 3 CYLD ablation induces migration capacity of SMZL cell lines. (A), (B) Expression levels of the CCR7 chemokine receptor were determined in two control (CTL) and two CYLD KO (KO) clones of SL-15 (A) and SL-22 (B) cell lines using flow cytometry. Values are presented as the mean \pm SEM of CD19⁺/CCR7⁺ percentages from at least three independent experiments. (C) Transendothelial migration analysis of one control (CTL) and two CYLD KO (KO) clones of SL-15 and SL-22 cell lines in the presence or absence of chemokines (CCL19 and CCL21) and after pre-incubation with anti-CCR7 antibody (CCR7 AB) or isotype control (IC). Values are shown as the mean \pm SEM of three independent experiments. (D), (E) RT-qPCR analysis of MMP9 mRNA expression in two control (CTL) and two CYLD KO (KO) clones of SL-15 (D) and SL-22 (E) cell lines. Values are shown as the mean \pm SEM of relative mRNA levels from at least three independent experiments. Data were normalized to MMP9 expression of control CTL-D4 or CTL-C9 clone. (F) Immunoblot analysis of (phosphorylated) AKT and (phosphorylated) ERK1/2 in whole cell extracts from two control (CTL) and two CYLD KO (KO) clones of SL-15 and SL-22 cell lines. Cells were pre-incubated with RPMI medium only or 10 μ g/mL isotype control antibody (IC) or 10 μ g/mL anti-CCR7 antibody for 30 min. Then, 200 ng/mL CCL19 was added for 5 min and whole cell extracts were collected. The picture is representative of three independent experiments. (G) One control (CTL) and two CYLD KO (KO) clones of the SL-15 SMZL cell line were injected intravenously in RAG2^{-/-} γ c^{-/-} immunodeficient mice and were sacrificed after 3 weeks. CD19⁺/CD45⁺ cells were detected by flow cytometry in the peripheral blood (PB), liver (LI), peritoneal cavity (PC), and spleen (SP), 3 weeks after intravenous injection. Values are shown as the mean \pm SEM of at least four mice. (H) Spleen weight analysis of at least four mice injected intravenously with one control (CTL) and two CYLD KO (KO) clones of SL-15 SMZL cell line and sacrificed after 3 weeks. Values are shown as the mean \pm SEM. (I) Representative picture of spleen analyzed in (I). (A)–(H) Statistical differences were assessed by Student's t-test (* p < 0.05; ** p < 0.01; *** p < 0.001).

the most significantly upregulated pathways in CYLD ablated cells (Supporting Information S1: Figure S5B), mirroring our in vitro results. Network biology analysis using the STRING database highlighted a protein-protein interaction graph (PPI) which contained, as the top-20 most central nodes, upregulated genes that are implicated in cell cycle progression (*CCDN1*^{27,28}), NF- κ B activation (*IL1B*²⁹) and increased motility (*FN1*³⁰, *IL6*³¹, *ICAM1*³²), as well as decreased tumor-suppressive genes like *PTEN* (Supporting Information S1: Figure S5C). Altogether, these findings support our in vitro functional results pointing to the same altered signaling pathways and biological processes.

MALT1-mediated cleavage of CYLD associates with CCR7-mediated migration of primary SMZL cells in vitro

To confirm the potential role of CYLD also in SMZL primary samples, we assessed CYLD protein expression levels in PBMCs and BMMCs

isolated from a cohort of 21 patients with SMZL. In 13/21 cases (61.9%), CYLD protein was fully cleaved by MALT1, as only the carboxyterminal (Ct) fragment of 70 kDa size was detected, while in the remaining 8 cases (38.1%) both the full length CYLD and the carboxyterminal (Ct) fragment were observed. Interestingly, all SMZL primary samples showed similar MALT1 protein levels (Figure 4A,B and Supporting Information S1: Figure S6A). Based on the full length CYLD expression status, cases were divided into CYLD^{full length} (cases with both full length CYLD and Ct fragment expression) and CYLD^{cleaved} (cases with only Ct fragment expression) subgroups. No clear correlation was observed between CYLD mRNA and protein levels, independently of the CYLD protein fragments detected (Supporting Information S1: Figure S6B).

In order to compare the activation status of the NF- κ B signaling pathway in the CYLD^{full length} versus the CYLD^{cleaved} subgroups, we checked the expression levels of known NF- κ B target genes, such as *CD80*, *IL6*, and *ICAM1*¹⁷ in isolated PBMCs and BMMCs. We observed higher expression levels of all NF- κ B target genes in CYLD^{cleaved} compared to CYLD^{full length} cases (*CD80*: P = 0.010; *IL6*:

$p=0.025$; ICAM1: $p=0.045$) (Supporting Information S1: Figure S6C–E). CYLD^{cleaved} patients showed more elevated CCR7 mRNA ($p=0.028$) and protein ($p=0.043$) levels compared to CYLD^{full length} patients (Figure 4C,D). Moreover, MMP9 mRNA was found

overexpressed in CYLD^{cleaved} patients ($p=0.007$) (Figure 4E). CYLD downregulation in CYLD^{full length} patient cells using the CRISPR/Cas9 system (Figure 4F,G) led to significant induction of all NF- κ B target genes, including CCR7 and MMP9 (Figure 4F). Transendothelial

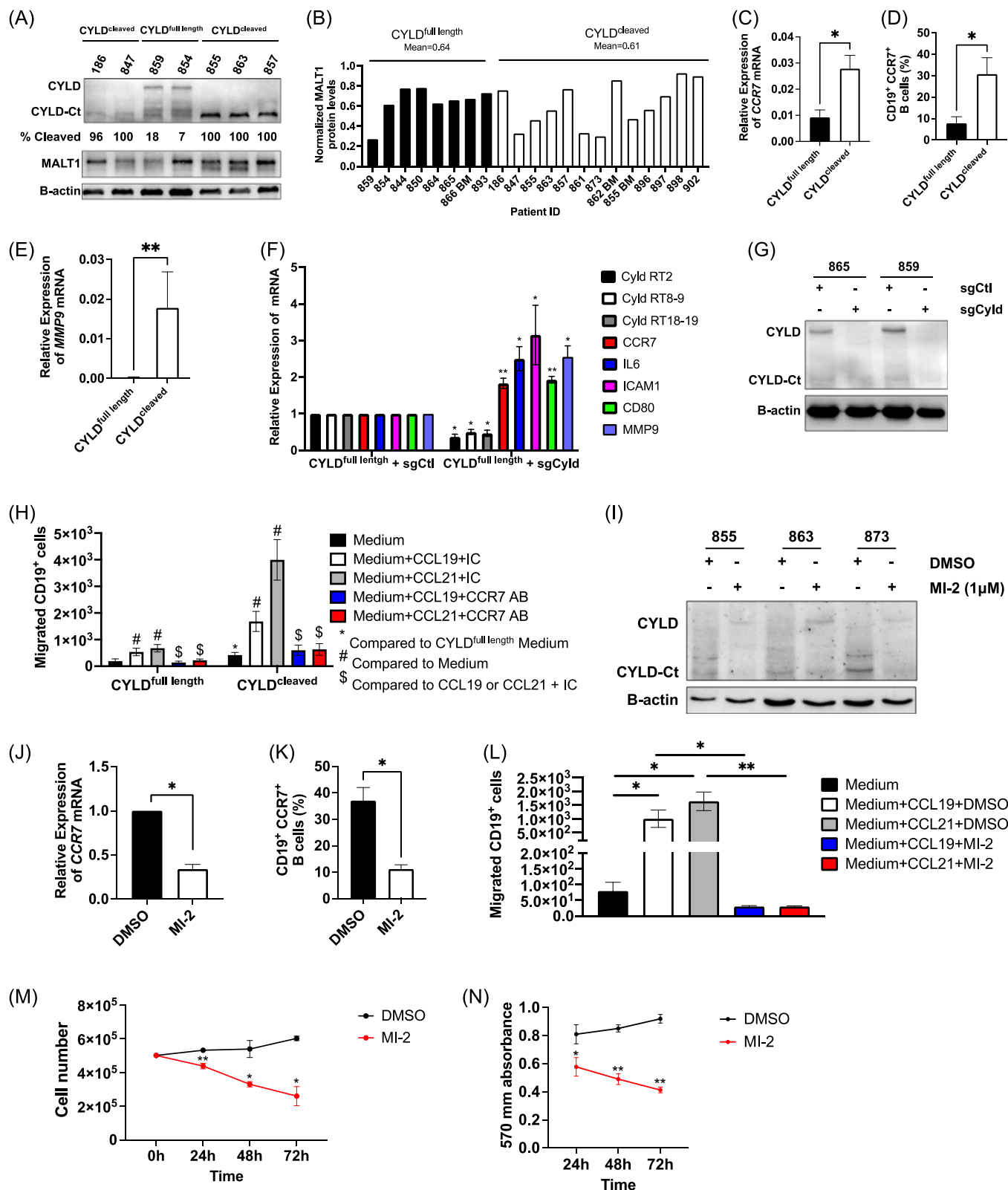


FIGURE 4 (See caption on next page).

FIGURE 4 MALT1-mediated cleavage of CYLD induces migration through the CCR7 receptor. (A) Immunoblot analysis of CYLD and MALT1 expression in primary SMZL samples. For CYLD analysis we used an antibody that recognizes both the full length CYLD and a C-terminal fragment of CYLD (CYLD-Ct). B-actin was used as a loading control. Representative picture of immunoblot analysis in 7 SMZL primary samples. (B) Quantification of MALT1 protein levels in patients with SMZL using the Image J software. Values are shown as the ratio of MALT1/B-actin for each patient. (C) RT-qPCR analysis of CCR7 mRNA expression in CYLD^{full length} and CYLD^{cleaved} subgroups. Values are shown as the mean \pm SEM of relative mRNA levels. (D) Expression levels of the CCR7 chemokine receptor were determined in CYLD^{full length} and CYLD^{cleaved} subgroups using flow cytometry. Values are shown as the mean \pm SEM of CD19⁺/CCR7⁺ percentages. (E) RT-qPCR analysis of MMP9 mRNA expression in CYLD^{full length} and CYLD^{cleaved} subgroups. Values are shown as the mean \pm SEM of relative mRNA levels. (F) Tumor cells from three SMZL patients expressing full length CYLD were electroporated with the CRISPR/Cas9 system including control (CYLD^{full length} + sgCtl) and CYLD-targeted (CYLD^{full length} + sgCyld) sgRNAs. RT-qPCR was used to analyze CYLD, CCR7, IL6, ICAM1, CD80, and MMP9 mRNA expression in CYLD^{full length} + sgCtl and CYLD^{full length} + sgCyld groups. Values are shown as the mean \pm SEM of relative mRNA levels. Data were normalized to mRNA expression of CYLD^{full length} + sgCtl group. (G) Representative immunoblot analysis of CYLD expression in tumor cells of samples analyzed in (F). (H) Transendothelial migration analysis of three CYLD^{full length} and CYLD^{cleaved} SMZL patient samples in the presence or absence of chemokines (CCL19 and CCL21) and after pre-incubation with anti-CCR7 antibody (CCR7 AB) or isotype control (IC). Values are shown as the mean \pm SEM. (I) Immunoblot analysis of CYLD expression in three CYLD^{cleaved} SMZL patients treated with DMSO (vehicle) or MALT1 inhibitor MI-2 (1 μ M) for 6 h. (J) RT-qPCR analysis of CCR7 mRNA expression in three CYLD^{cleaved} SMZL patients treated with DMSO (vehicle) or MALT1 inhibitor MI-2 (1 μ M) for 24 h. Values are shown as the mean \pm SEM of relative mRNA levels. (K) Expression levels of the CCR7 chemokine receptor were determined in three CYLD^{cleaved} SMZL patients treated with DMSO (vehicle) or MALT1 inhibitor MI-2 (1 μ M) for 24 h, using flow cytometry. Values are shown as the mean \pm SEM of CD19⁺/CCR7⁺ percentages. (L) Transendothelial migration analysis of three CYLD^{cleaved} SMZL patients in the presence of CCL19 and CCL21 chemokines, after pre-incubation with DMSO (vehicle) or MALT1 inhibitor MI-2 (1 μ M) for 6 h. Values are shown as the mean \pm SEM. (M), (N) Proliferation analysis by Trypan blue exclusion assay (M) and MTT assay (N) of three CYLD^{cleaved} SMZL patients treated with DMSO (vehicle) or MALT1 inhibitor MI-2 (1 μ M) for, 24, 48, and 72 h. Values are shown as the mean \pm SEM. (C)–(N) Statistical differences were assessed by Student's *t*-test (*, #, \$*p* < 0.05; ***p* < 0.01).

transwell migration assay revealed a higher migration capacity of cells from CYLD^{cleaved} patients in the absence of chemoattractant stimuli. Addition of CCL19/CCL21 ligands induced migration in all cases, albeit this effect was more pronounced in CYLD^{cleaved} patients (transendothelial migration assay after CCL19 addition: CYLD^{full length}, from 0.2×10^3 to 0.5×10^3 ; CYLD^{cleaved}, from 0.4×10^3 to 1.7×10^3). Previous incubation with an anti-CCR7 antibody impaired the migration ability of primary cells from both CYLD^{full length} and CYLD^{cleaved} patients, similar to basal levels (Figure 4H). Altogether, our findings suggest that full length CYLD represses the migration capacity of SMZL cells through suppression of the NF- κ B/CCR7 axis.

To justify the direct effect of MALT1 proteolytic activity on CYLD in patients with SMZL, CYLD^{cleaved} patient cells were treated with the MALT1 inhibitor MI-2 leading to a clear reduction of the carboxyterminal (Ct) fragment along with a concomitant increase of full length CYLD levels (Figure 4I). Moreover, MI-2 treatment diminished CCR7 expression (Figure 4J) as well as CCR7 protein levels (Figure 4K). Interestingly, previous incubation of CYLD^{cleaved} patient cells with the MI-2 inhibitor completely restrained their transendothelial migration capacity (Figure 4L). In addition, CYLD^{cleaved} patient cells showed significantly reduced cell growth after MALT1 inhibition (Figure 4M,N).

CYLD deletion activates BcR signaling and induces resistance to ibrutinib

To investigate the role of CYLD in BcR signaling, we assessed the activation status of downstream key molecules in CYLD KO and control SL-15 and SL-22 cells. We found that CYLD KO was associated with the activation of BcR signaling as indicated by increased phosphorylation of BTK and downstream AKT and ERK1/2 (Figure 5A). Prompted by these findings, we used the BTK inhibitor ibrutinib to evaluate the possibility of modulating BcR signaling. When the parental SL-15 and SL-22 cell lines were exposed to different concentrations of ibrutinib (1–20 μ M) for 72 h, we observed a progressive decrease of cell viability in a dose-dependent manner.

The two cell lines differed in terms of IC₅₀ value with the SL-22 cell line showing a significantly higher value (Trypan Blue: 9.83 μ M and CellTiter-Glo: 11.18 μ M) compared to the SL-15 cell line (Trypan Blue: 2.79 μ M and CellTiter-Glo: 5.85 μ M) (Figure 5B). We then

treated both control and CYLD KO clones of the SL-15 cell line with 2.5 μ M and 5 μ M of ibrutinib for up to 72 h. CYLD KO clones appeared to be more resistant to the proliferation repression by ibrutinib compared to control clones (5 μ M ibrutinib CellTiter-Glo; CTL D4: 63.3%, CTL D6: 65.7%, KO E2: 75.8% and KO H11: 79.9%) (Figure 5C,D and Supporting Information S1: Figure S7A,B). In similar experiments, CYLD KO SL-22 cells showed resistance to proliferation repression after 10 μ M ibrutinib treatment for up to 72 h (Figure 5E,F).

Cell mobilization is a well-known effect of ibrutinib treatment, reported in CLL³³ and MCL.³⁴ To study how ibrutinib affects SMZL cell mobilization in vitro, we adapted the 3D model previously validated for CLL,^{35,36} in which SMZL cells were seeded together with HS-5 bone marrow stromal cells in gelatin sponge scaffolds (SpongostanTM) and cultured under dynamic conditions in a rotary cell culture system (RCCSTM). CTL and CYLD KO clones were seeded in the scaffolds and cultured in the presence of 5 μ M ibrutinib for 16 h. CYLD KO cells (KO H11) showed reduced egress from the scaffold compared to CTL cells (CTL D4) (Figure 5G,H), further implicating CYLD in resistance to ibrutinib.

DISCUSSION

Our study provides evidence that the functional loss of the CYLD gene is implicated in the pathophysiology of SMZL^{13,17} and that decreased CYLD expression is associated with worse 10-year relative survival. This is in line with evidence from other B cell lymphomas, including DLBCL, MCL, and CLL, where low CYLD expression has been correlated with worse prognosis^{13,17} highlighting the need for further investigation into how CYLD dysregulation is implicated in the natural history of these entities. In that regard, the miR-17–92 cluster has been reported to promote lymphoma development in mice that resemble human lymphomas by targeting CYLD among others.³⁷ Moreover, CYLD was among several tumor suppressor genes that were re-expressed after pharmacological inhibition of methylation in SMZL cell lines.³⁸

Here we report that the ablation of CYLD in SMZL cells has relevant functional consequences particularly associated with a more aggressive phenotype.^{21,22} CYLD KO cells displayed activation of both the canonical and the non-canonical NF- κ B signaling pathways

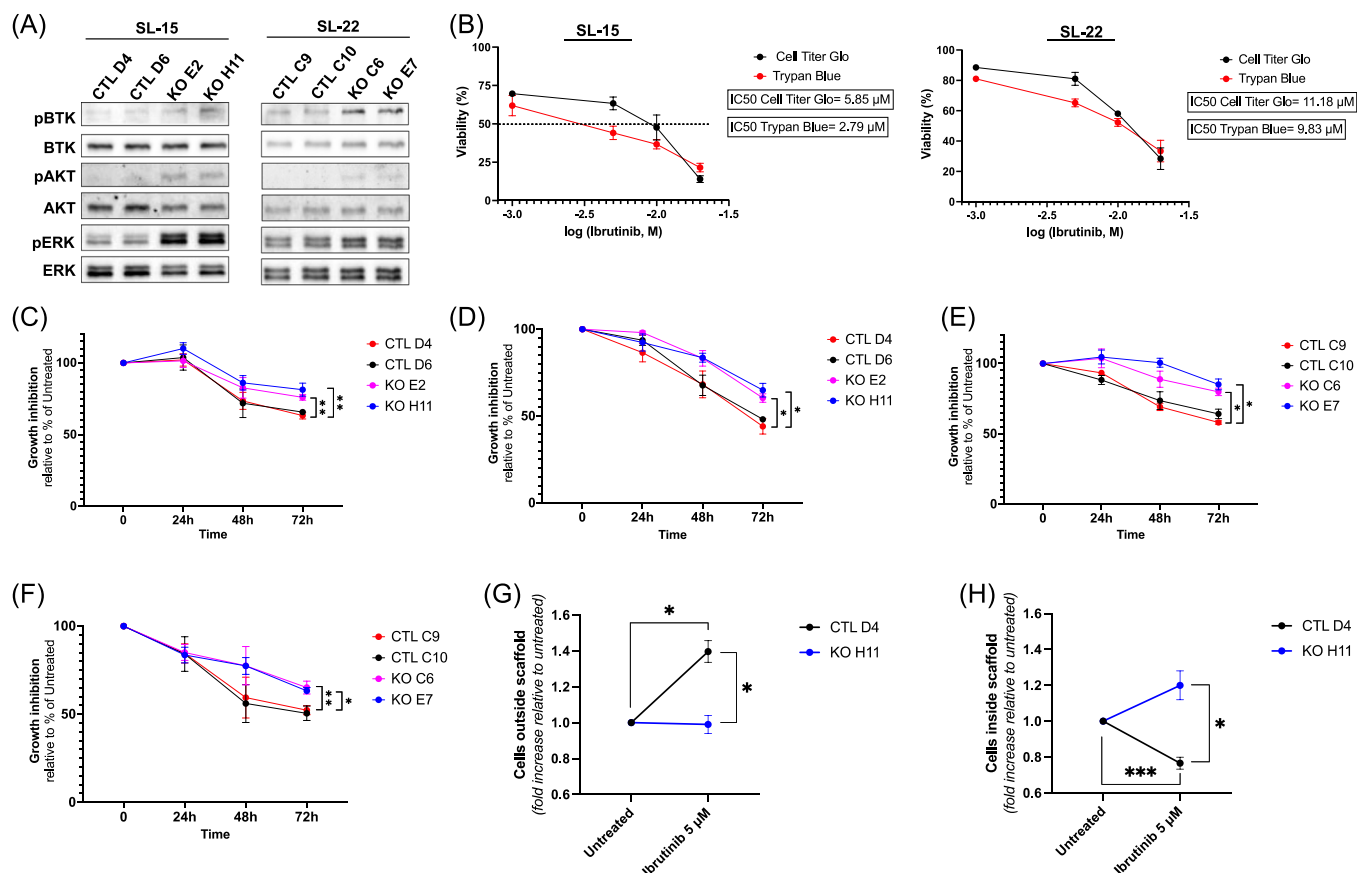


FIGURE 5 CYLD ablation induces Bcr signaling pathway activation and confers resistance to Ibrutinib. **(A)** Immunoblot analysis of (phosphorylated) BTK, (phosphorylated) AKT, and (phosphorylated) ERK1/2 in whole cell extracts from two control (CTL) and two CYLD KO (KO) clones of SL-15 and SL-22 cell lines. The picture is representative of three independent experiments. **(B)** Parental SL-15 and SL-22 cell lines were treated with different ibrutinib concentrations (1, 2.5, 5, 10, and 20 μM) for 72 h, and viability was assessed by Trypan Blue exclusion and CellTiter Glo assay. IC_{50} value was calculated using a nonlinear regression tool from GraphPad Prism Version 9 software. **(C)**, **(D)** Two control (CTL) and two CYLD KO (KO) clones of the SL-15 cell line were grown in the presence or absence of 5 μM ibrutinib for 24, 48, and 72 h. Proliferation analysis was assessed by CellTiter-Glo **(C)** and Trypan blue exclusion **(D)** assays. The percentage of growth inhibition was calculated by the ratio between the number of live cells treated and the number of live cells of the respective vehicle (DMSO). Values are shown as the mean \pm SEM of triplicate experiments and were analyzed by Student's *t*-test (* $p < 0.05$, ** $p < 0.01$). **(E)**, **(F)** Two control (CTL) and two CYLD KO (KO) clones of the SL-22 cell line were grown in the presence or absence of 10 μM ibrutinib for 24, 48, and 72 h. Proliferation analysis was assessed by CellTiter-Glo **(E)** and Trypan blue exclusion **(F)** assays. The percentage of growth inhibition was calculated by the ratio between the number of live cells treated and the number of live cells of the respective vehicle (DMSO). Values are shown as the mean \pm SEM of triplicate experiments and were analyzed by Student's *t*-test (* $p < 0.05$, ** $p < 0.01$). **(G)**, **(H)** SL-15 CTL D4 and CYLD KO H11 cell lines were used to populate a spongostan scaffold and subsequently treated with ibrutinib. Line plot represents the number of cells mobilized **(G)** or remaining within the scaffolds **(H)**, 16 h after the addition of ibrutinib compared to untreated cells. Values are presented as the mean \pm SEM. Statistical differences were assessed by two-way ANOVA followed by Fisher's test (* $p < 0.05$, *** $p < 0.001$).

that correlated with higher proliferation and cell cycle progression. These findings are in agreement with a previously performed microarray and qPCR analysis, using the primary PB-15 and PB-22 cells as well as the derived SL-15 and SL-22 cell lines, demonstrating upregulation of genes that control mitosis and cell proliferation, such as *PLK1*, *CDK1*, and *CDK2*, in the relapsed/refractory phase.²² Moreover, CYLD ablation induced Bcr signaling activation, as attested by elevated BTK phosphorylation at Tyr223 as well as activation of the downstream PI3K/AKT and MEK/ERK signaling pathways³⁹ in CYLD KO clones. This unexpected finding indicates a possible role of CYLD upstream of BTK and not downstream as already demonstrated in other types of B-cell lymphoma,^{16,17} opening the path to alternative modalities to inhibit Bcr signaling, a key mechanism of lymphoma-genesis in general. Interestingly, CYLD ablation appeared to be associated with ibrutinib resistance in vitro, as previously reported for aggressive Bcr-dependent B cell lymphomas.¹⁷ Of note, we observed

such resistance, in our in vitro 3D model, even at micromolar concentrations of the drug that are not typically achieved in vivo in the clinical setting due to the possibility of off-target effects in patients. This molecular mechanism of resistance is of particular interest in SMZL, given the rather limited efficacy of ibrutinib in SMZL⁴⁰ and the possibility that interfering with CYLD signaling might help boost the response to BTK inhibitors.

Among the known NF- κB target genes is *CCR7*,²⁵ which encodes for the G-protein coupled receptor CCR7. It enables normal lymphocytes to access secondary lymphoid tissues, such as the lymph nodes or the spleen.^{41,42} CYLD ablation upregulated CCR7 expression levels in SMZL cells, through NF- κB hyperactivation, and simultaneously increased their migration capacity. This was associated with increased ERK1/2 and AKT activation downstream of the CCR7 receptor, further augmented upon ligand binding in CYLD ablated cells. Of note, in vivo studies showed that CYLD KO clones

accumulated more efficiently in all analyzed compartments with increased splenomegaly with tumor foci, thus correlating with a more aggressive disease. This finding might be explained by an increased dissemination capacity *in vitro* in keeping with the increased chemokines-responsiveness shown *in vitro*. Alternatively, the observed expansion in the tissues can be also interpreted as a consequence of the higher cell growth capacity, as exhibited by CYLD KO clones *in vitro*.

BcR activation leads to the formation of a CARD11–BCL10–MALT1 (CBM) signaling complex that activates the canonical NF-κB signaling pathway, through MALT1-mediated proteolytic cleavage of NF-κB negative regulators, such as CYLD and A20.^{17,43–46} CYLD is cleaved by MALT1 and both the C-terminal and N-terminal fragments are rapidly degraded by the proteasome, leading to CYLD inactivation.¹⁷ In our cohort of SMZL primary samples, we identified two distinct groups, CYLD^{full length} and CYLD^{cleaved} cases, based on the CYLD full length expression status. CYLD^{cleaved} patients showed higher canonical NF-κB signaling, assessed by upregulation of known NF-κB target genes, such as *CD80*, *IL6*, *ICAM1*, and *CCR7*. The latter appeared relevant for the basal increased transendothelial migration capacity of CYLD^{cleaved} cases by upregulating also the *MMP9* gene. CCL19/CCL21 binding augmented migration in both CYLD^{full length} and CYLD^{cleaved} cases; however, the effect was more pronounced in the latter. Interestingly, downregulation of CYLD in CYLD^{full length} samples, induced canonical NF-κB signaling activation.

In a preliminary analysis of 21 cases, patients carrying cleaved form of CYLD were significantly younger at SMZL diagnosis compared to the CYLD^{full length} subgroup (62.9 vs. 75.4 years). Importantly, patients of the CYLD^{cleaved} subgroup, characterized by aggressive disease, presented also a significantly decreased absolute lymphocyte number (ALC: $48.9 \times 10^9/L$ vs. $189.2 \times 10^9/L$, $p = 0.002$), higher spleen enlargement (28.2 vs. 21.6 cm, $p = 0.042$), and a trend to lower BM involvement (47.5% vs. 66.7%, $p = 0.33$) compared to CYLD^{full length} cases. Interestingly, a higher percentage of patients of CYLD^{cleaved} subgroup (6/13, 46.1%) needed treatment compared to patients of CYLD^{full length} subgroup (3/8, 37.5%) despite similar follow-up (average follow-up time; CYLD^{full length}: 3.07 ± 1.49 years and CYLD^{cleaved}: 3.16 ± 1.77 years). Interestingly, only 1 of 21 patients was lost during the follow-up, after the transformation of SMZL to DLBCL, and this case belonged to the CYLD^{cleaved} subgroup.

Admittedly, these results warrant further analysis and confirmation in larger cohorts of patients, yet they support a potential critical role for CYLD in the progression and aggressiveness of SMZL also in the clinical setting.

Taken together, our results underscore the key role of CYLD in SMZL pathogenesis through the multimodal regulation of NF-κB and BcR downstream signaling pathways, leading to a more disseminated and aggressive disease. These findings may explain the relative resistance of SMZL to first-generation BTK inhibitors, thus providing novel insights for the development of innovative combination therapeutic strategies, by targeting the CCR7–MALT1 pathways.

ACKNOWLEDGMENTS

Open access funding provided by BIBLIOSAN.

AUTHOR CONTRIBUTIONS

Athanasios Pseftogas, Konstantinos Xanthopoulos, and Paolo Ghia designed the study. Athanasios Pseftogas, Jessica Bordini, Silvia Heltai, Caterina Taccetti, Pamela Ranghetti, and Eleonora Perotta performed the experiments. Manasori Daibata and José Ángel Martínez Climent contributed SMZL cell lines. Davide Rossi provided RNA-seq data from SMZL patients. Ferdinando Bonfiglio, Georgios Gavrilidis, Sofoklis Keisaris, and Vasileios Vasileiou performed the

bioinformatic analysis. Elisa Albi, Francesca Martini, Emmanuela Sant'Antonio, Fabrizio Mavilia, and Lydia Scarfò provided patient specimens and clinical information. Athanasios Pseftogas acquired funding. Paolo Ghia supervised most experiments and the overall implementation of the study and acquired funding. Athanasios Pseftogas, Jessica Bordini, Ferdinando Bonfiglio, Georgios Gavrilidis, Michela Frenquelli, Alessandro Campanella, Konstantinos Xanthopoulos, and Paolo Ghia interpreted data and wrote the manuscript. Paolo Ghia, Kostas Stamatopoulos, and Lydia Scarfò revised the manuscript. All authors analyzed data and reviewed and approved the final version of the manuscript.

CONFLICT OF INTEREST STATEMENT

Paolo Ghia: honoraria/advisory board: AbbVie, AstraZeneca, BeiGene, BMS, Galapagos, Janssen, Loxo/Lilly, MSD, Roche; research funding: AbbVie, AstraZeneca, BMS, Janssen; Kostas Stamatopoulos: honoraria/advisory board: AbbVie, AstraZeneca, Gilead, Janssen; research funding: AbbVie, Gilead, Janssen; José Ángel Martínez Climent: research funding: AstraZeneca, BMS-Celgene, Janssen, Palleon, Roche-Genentech; Davide Rossi: honoraria/research funding: AbbVie, AstraZeneca; Cellectia, Gilead, Janssen, Verastem, Roche; Lydia Scarfò: advisory board: AbbVie, AstraZeneca, Janssen.

DATA AVAILABILITY STATEMENT

RNA-seq data may be found at the European Nucleotide Archive (ENA), <https://www.ebi.ac.uk/ena/browser/home> under accession number PRJEB75539. For more details, contact A. Pseftogas.

FUNDING

The research leading to these results has received funding from International Cancer Research Fellowships–2 (i-CARE2) co-funded by the AIRC Foundation for Cancer Research (AIRC) and the European Union, under the Marie Skłodowska-Curie Action H2020-MSCA-COFUND-2017, grant agreement No 800 924. This research was also supported by the AIRC Italy Postdoc 2022 Fellowship in the memory of Professor Ugo Mario Cazzani and AIRC IG 2017–ID. 20 246–P.I. Ghia Paolo, IG 2022–ID. 27 566, P.I. Ghia Paolo and under 5 per Mille 2018 –ID. 21 198 program–P.I. Foà Roberto, G.L. Ghia Paolo; Towards Precision Medicine: Advanced cellular analytics in biomedical research–PureCell, funded by the Hellenic Foundation for Research and Innovation (K.S.).

ORCID

Athanasios Pseftogas  <http://orcid.org/0000-0002-6165-8119>

Paolo Ghia  <http://orcid.org/0000-0003-3750-7342>

SUPPORTING INFORMATION

Additional supporting information can be found in the online version of this article.

REFERENCES

1. Armitage JO, Weisenburger DD. New approach to classifying non-Hodgkin's lymphomas: clinical features of the major histologic subtypes. Non-Hodgkin's Lymphoma Classification Project. *J Clin Oncol*. 1998;16(8):2780–2795.
2. Martínez N, Almaraz C, Vaqué JP, et al. Whole-exome sequencing in splenic marginal zone lymphoma reveals mutations in genes involved in marginal zone differentiation. *Leukemia*. 2014;28(6):1334–1340.

3. Rossi D, Trifonov V, Fangazio M, et al. The coding genome of splenic marginal zone lymphoma: activation of NOTCH2 and other pathways regulating marginal zone development. *J Exp Med*. 2012;209(9):1537-1551.
4. Clipson A, Wang M, de Leval L, et al. KLF2 mutation is the most frequent somatic change in splenic marginal zone lymphoma and identifies a subset with distinct genotype. *Leukemia*. 2015;29(5):1177-1185.
5. Bikos V, Darzentas N, Hadzidimitriou A, et al. Over 30% of patients with splenic marginal zone lymphoma express the same immunoglobulin heavy variable gene: Ontogenetic implications. *Leukemia*. 2012;26(7):1638-1646.
6. Fonte E, Agathangelidis A, Reverberi D, et al. Toll-like receptor stimulation in splenic marginal zone lymphoma can modulate cell signaling, activation and proliferation. *Haematologica*. 2015;100(11):1460-1468.
7. Parry M, Rose-Zerilli MJ, Ljungström V, et al. Genetics and Prognostication in Splenic Marginal Zone Lymphoma: Revelations from Deep Sequencing. *Clin Cancer Res*. 2015;21(18):4174-4183.
8. Bonfiglio F, Brusca G, Guidetti F, et al. Genetic and phenotypic attributes of splenic marginal zone lymphoma. *Blood*. 2022;139(5):732-747.
9. Niu J, Shi Y, Iwai K, Wu ZH. LUBAC regulates NF- κ B activation upon genotoxic stress by promoting linear ubiquitination of NEMO. *EMBO J*. 2011;30(18):3741-3753.
10. Hellerbrand C, Bumes E, Bataille F, Dietmaier W, Massoumi R, Bosserhoff AK. Reduced expression of CYLD in human colon and hepatocellular carcinomas. *Carcinogenesis*. 2007;28(1):21-27.
11. Massoumi R, Kuphal S, Hellerbrand C, et al. Down-regulation of CYLD expression by Snail promotes tumor progression in malignant melanoma. *J Exp Med*. 2009;206(1):221-232.
12. Bignell GR, Warren W, Seal S, et al. Identification of the familial cylindromatosis tumour-suppressor gene. *Nat Genet*. 2000;25(2):160-165.
13. Wu W, Zhu H, Fu Y, et al. Clinical significance of down-regulated cylindromatosis gene in chronic lymphocytic leukemia. *Leuk Lymphoma*. 2014;55(3):588-594.
14. Schmidt A, Schmitz R, Giefing M, et al. Rare occurrence of biallelic CYLD gene mutations in classical Hodgkin lymphoma. *Genes Chromosom Cancer*. 2010;49(9):803-809.
15. Annunziata CM, Davis RE, Demchenko Y, et al. Frequent engagement of the classical and alternative NF- κ B pathways by diverse genetic abnormalities in multiple myeloma. *Cancer Cell*. 2007;12(2):115-130.
16. McAllister-Lucas LM, Baens M, Lucas PC. MALT1 protease: a new therapeutic target in B lymphoma and beyond? *Clin Cancer Res*. 2011;17(21):6623-6631.
17. Minderman M, Lantermans HC, Grüneberg LJ, et al. MALT1-dependent cleavage of CYLD promotes NF- κ B signaling and growth of aggressive B-cell receptor-dependent lymphomas. *Blood Cancer J*. 2023;13(1):37.
18. Xu X, Wei T, Zhong W, et al. Down-regulation of cylindromatosis protein phosphorylation by BTK inhibitor promotes apoptosis of non-GCB-diffuse large B-cell lymphoma. *Cancer Cell Int*. 2021;21(1):195.
19. Spina V, Mensah AA, Arribas AJ. Biology of splenic and nodal marginal zone lymphomas. *Ann Lymphoma*. 2021;5:6.
20. Arcaini L, Rossi D. Nuclear factor- B dysregulation in splenic marginal zone lymphoma: new therapeutic opportunities. *Haematologica*. 2012;97(5):638-640.
21. Daibata M, Taguchi T, Nemoto Y, Iwasaki S, Ohtsuki Y, Taguchi H. In vitro Epstein-Barr virus-immortalized lymphoma cell line carrying t(9;14)(p13;q32) chromosome abnormality, derived from splenic lymphoma with villous lymphocytes. *Int J Cancer*. 2006;118(2):513-517.
22. Higuchi T, Hashida Y, Taniguchi A, Kamioka M, Daibata M. Differential gene expression profiling linked to tumor progression of splenic marginal zone lymphoma. *Sci Rep*. 2017;7(1):11026.
23. Pseftogas A, Xanthopoulos K, Poutahidis T, et al. The tumor suppressor CYLD inhibits mammary epithelial to mesenchymal transition by the coordinated inhibition of YAP/TAZ and TGF β signaling. *Cancers*. 2020;12(8):2047.
24. Ederer F, Heise H. Instructions to IBM 650 programmers in processing survival computations. Methodological Note no. 10, End Results Evaluation Section. Technical Report. Bethesda, MD: National Cancer Institute; 1959.
25. Mburu YK, Egloff AM, Walker WH, et al. Chemokine receptor 7 (CCR7) gene expression is regulated by NF- κ B and activator protein 1 (AP1) in metastatic squamous cell carcinoma of head and neck (SCCHN). *J Biol Chem*. 2012;287(5):3581-3590.
26. Cuesta-Mateos C, López-Giral S, Alfonso-Pérez M, et al. Analysis of migratory and prosurvival pathways induced by the homeostatic chemokines CCL19 and CCL21 in B-cell chronic lymphocytic leukemia. *Exp Hematol*. 2010;38(9):756-764.e4.
27. Musgrove EA, Lee CS, Buckley MF, Sutherland RL. Cyclin D1 induction in breast cancer cells shortens G1 and is sufficient for cells arrested in G1 to complete the cell cycle. *Proc Natl Acad Sci USA*. 1994;91(17):8022-8026.
28. Guardavaccaro D, Corrente G, Covone F, et al. Arrest of G₁-S progression by the p53-inducible gene PC3 is Rb dependent and relies on the inhibition of cyclin D1 transcription. *Mol Cell Biol*. 2000;20(5):1797-1815.
29. Lawrence T, Gilroy DW, Colville-Nash PR, Willoughby DA. Possible new role for NF- κ B in the resolution of inflammation. *Nat Med*. 2001;7(12):1291-1297.
30. Cai X, Liu C, Zhang TN, Zhu YW, Dong X, Xue P. Down-regulation of FN1 inhibits colorectal carcinogenesis by suppressing proliferation, migration, and invasion. *J Cell Biochem*. 2018;119(6):4717-4728.
31. SUN W, LIU D-B, LI W-W, et al. Interleukin-6 promotes the migration and invasion of nasopharyngeal carcinoma cell lines and upregulates the expression of MMP-2 and MMP-9. *Int J Oncol*. 2014;44(5):1551-1560.
32. Millán J, Hewlett L, Glyn M, Toomre D, Clark P, Ridley AJ. Lymphocyte transcellular migration occurs through recruitment of endothelial ICAM-1 to caveola- and F-actin-rich domains. *Nat Cell Biol*. 2006;8(2):113-123.
33. Wodarz D, Garg N, Komarova NL, et al. Kinetics of CLL cells in tissues and blood during therapy with the BTK inhibitor ibrutinib. *Blood*. 2014;123(26):4132-4135.
34. Chang BY, Francesco M, De Rooij MFM, et al. Egress of CD19⁺ CD5⁺ cells into peripheral blood following treatment with the Bruton tyrosine kinase inhibitor ibrutinib in mantle cell lymphoma patients. *Blood*. 2013;122(14):2412-2424.
35. Belloni D, Ferrarini M, Ferrero E, et al. Protocol for generation of 3D bone marrow surrogate microenvironments in a rotary cell culture system. *STAR Protoc*. 2022;3(3):101601.
36. Federica Barbaglio B, Daniela Belloni B, Lydia Scarfò S, et al. Three-dimensional co-culture model of chronic lymphocytic leukemia bone marrow microenvironment predicts patient-specific response to mobilizing agents. *Haematologica*. 2020;106(9):2334-2344.
37. Jin HY, Oda H, Lai M, et al. MicroRNA-17~92 plays a causative role in lymphomagenesis by coordinating multiple oncogenic pathways. *EMBO J*. 2013;32(17):2377-2391.
38. Arribas AJ, Rinaldi A, Mensah AA, et al. DNA methylation profiling identifies two splenic marginal zone lymphoma subgroups with different clinical and genetic features. *Blood*. 2015;125(12):1922-1931.

39. Efremov DG, Turkalj S, Laurenti L. Mechanisms of B cell receptor activation and responses to B cell receptor inhibitors in B cell malignancies. *Cancers*. 2020;12(6):1396.
40. Noy A, de Vos S, Thieblemont C, et al. Targeting Bruton tyrosine kinase with ibrutinib in relapsed/refractory marginal zone lymphoma. *Blood*. 2017;129(16):2224-2232.
41. Rehm A, Mensen A, Schrödi K, et al. Cooperative function of CCR7 and lymphotoxin in the formation of a lymphoma-permissive niche within murine secondary lymphoid organs. *Blood*. 2011;118(4):1020-1033.
42. Förster R, Schubel A, Breitfeld D, et al. CCR7 coordinates the primary immune response by establishing functional micro-environments in secondary lymphoid organs. *Cell*. 1999;99(1):23-33.
43. Klei LR, Hu D, Panek R, et al. MALT1 protease activation triggers acute disruption of endothelial barrier integrity via CYLD cleavage. *Cell Rep*. 2016;17(1):221-232.
44. Coornaert B, Baens M, Heyninck K, et al. T cell antigen receptor stimulation induces MALT1 paracaspase-mediated cleavage of the NF- κ B inhibitor A20. *Nat Immunol*. 2008;9(3):263-271.
45. Thome M. CARMA1, BCL-10 and MALT1 in lymphocyte development and activation. *Nat Rev Immunol*. 2004;4(5):348-359.
46. Blonska M, Lin X. CARMA1-mediated NF- κ B and JNK activation in lymphocytes. *Immunol Rev*. 2009;228(1):199-211.